Appl Phys B (2011) 102: 381–389
DOI 10.1007/s00340-010-4011-0

Applied Physics B
Lasers and Optics

VCSEL-based calibration-free carbon monoxide sensor at 2.3 µm with in-line reference cell

J. Chen · A. Hangauer · R. Strzoda · M.-C. Amann

Received: 3 December 2009 / Revised version: 5 March 2010 / Published online: 28 April 2010

Abstract A compact and calibration-free carbon monoxide sensor approach utilizing the wide current-tunability of 2.3 µm VCSELs is reported. A separate reference cell is avoided by filling the reference gas (methane) in the photodetector housing. By applying bandwidth optimized wide/narrow wavelength scan concept, inherent wavelength scale calibration and self-monitoring of the sensor are realized, with which the laser aging process is also under control. An efficient linear least-squares curve fit using an analytical signal model for the narrow scan spectrum is done, utilizing the knowledge of the absolute wavelength scale and also the estimated WMS modulation amplitude obtained from the wide scan. The scan width of the narrow spectrum is optimized aiming at the maximum signal to noise ratio on the determined CO concentration. These concepts are universal and can be utilized for optical sensing of other gases as well and the sensor was tested under diverse applications e.g. fire detection and combustion optimization.

1 Introduction

Carbon monoxide (CO) is a toxic gas, which affects human health whenever present in the ambient air. CO escaping from home burners is the most frequent cause for unintentional death at home with a death toll of annually 500 persons in the USA [1]. Moreover, it is the most prominent gas to be detected for gas sensor based fire detection [2]. The requirements for such sensors are compactness, long-term stability, high sensitivity (ppm range) and selectivity, and highest possible reliability.

Diverse CO measurements were carried out by different groups either at environmental condition [3, 4] or in combustion [5–7] applying Tunable Diode Laser Absorption Spectroscopy (TDLAS) using edge-emitting laser diodes. However, the measurement configurations are rather complex. In this paper, a light-weight and small sensor concept (optical cell: ≈7 cm overall extent feasible) capable of CO detection in ppm range with 1 Hz bandwidth is reported. It is based on TDLAS utilizing unique advantages of Vertical-Cavity Surface-Emitting Lasers (VCSELs). No separate gas reference cell is needed. It marks an important technological step in CO sensing providing a reliable, cost-efficient and mobile solution for toxic gas monitoring.

We present a system-inherent wavelength calibration technique with a reference gas in the measurement optical path, which reduces the complexity of the conventional sensor concept with separate reference cell. Additionally, identification of the CO absorption line and determination of the CO concentration are performed automatically by employing an efficient wide/narrow scan concept. Wide wavelength tuning of several nm via current allows for determination of the wavelength scale by adjacent methane absorption lines, which enables an efficient curve fit in the narrow spectrum scan around the CO line. This method requires sufficiently wide current-tunable lasers like VCSELs ($\Delta\lambda > 4$ nm). Such performance cannot be achieved by conventional 2.3 µm edge-emitting DFB lasers ($\Delta\lambda <$ 2.1 nm) [8]. Due to the wide wavelength scan of about 3 nm, the nonlinearity of the current to wavelength scale reveals important. It is taken into account for accurate determina-

J. Chen (✉) · A. Hangauer · R. Strzoda
Corporate Technology, Siemens AG, Otto-Hahn-Ring 6, 80200 Munich, Germany
e-mail: jia.chen@wsi.tum.de

J. Chen · A. Hangauer · M.-C. Amann
Walter Schottky Institute, Technical University of Munich, Am Coulombwall 3, 85748 Garching, Germany

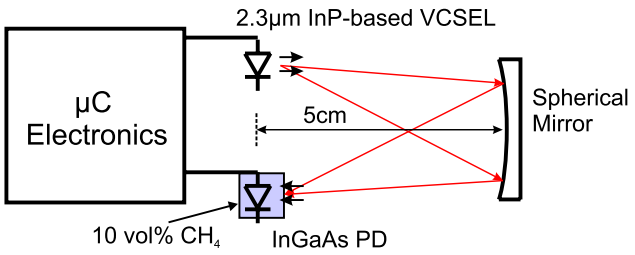

Fig. 1 Schematic design of the CO sensor: a compact absorption cell with 2×5 cm optical path length (reflective geometry) is used in combination with microprocessor controlled electronics (board dimensions: 10 cm×10 cm). 10 vol% reference gas (CH_4) is filled in the photodetector housing and therefore directly integrated in the measurement optical path

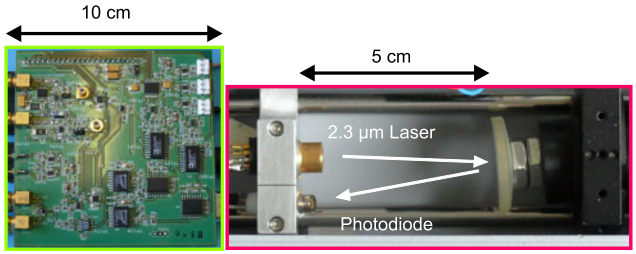

Fig. 2 Photograph of the absorption cell and the microprocessor controlled electronics

tion of the position of the CO absorption line as well as the wavelength modulation amplitude, which is bias current dependent. Moreover, the width of the narrow spectrum scan is chosen optimally to achieve the highest possible signal to noise ratio (SNR) on the concentration values and thus maximized sensor sensitivity. For this, the theoretical sensor model and experimental results are in good agreement.

2 Optical cell design

To reliably measure trace gas concentrations with TDLAS, exact knowledge of the scanned absolute wavelength scale is needed. Because CO is a trace gas, the measured gas absorption spectrum in ambient air has no indication of the CO absorption line position. Furthermore, the VCSEL current to wavelength relationship and its dependency on modulation frequency are not exactly known and cannot be assumed to be constant for long-term stable sensor operation. The nonlinear current to wavelength tuning behavior may change when the laser ages. Therefore, the laser current used to scan the CO absorption line cannot be determined a priori even though the wavelength position of the absorption line is known from the HITRAN database [9].

Conventionally, line locking is used to lock the wavelength position of the laser to the absorption line of interest: the laser beam is split and passed through the main absorption cell and in parallel through a separate reference cell, which contains the target gas in a high concentration [5]. To reduce the complexity of the measurement cell, we follow a different approach by including methane (CH_4) in the photodetector housing, i.e. in the optical path of the absorption cell. Because methane has absorption lines in the same wavelength range as carbon monoxide, it can be used as a reference gas. In Fig. 1 and Fig. 2, the compact design of the CO sensor is shown. To accomplish a defined methane absorbance of $2.5 \cdot 10^{-3}$, a reference gas containing 10% CH_4 is included in the cap of the photodetector forming an optical absorption path of about 0.6 mm. Since methane is not the target gas, limited outdiffusion of methane during the life time does not affect the lower detection limit of CO. Moreover, leaking of methane can be detected in the wide spectrum scan. Recently developed 2.3 µm InP-based VCSELs [10, 11] with a current tuning coefficient of around 1.1 nm/mA (2.0 cm^{-1}/mA) were used in this sensor. Single-mode GaSb-based VCSELs at 2.3 µm [12] could be alternatively used. A spherical mirror is used to focus the light on the detector and to extend the absorption path length to 10 cm. The laser can has no window and the photodiode is tilted to avoid fringes. A compact, microcontroller-based electronics (board dimensions: 10 cm × 10 cm) serves as sensor control, signal processing and data evaluation. The current of the laser device is tuned periodically to scan the absorption spectrum and the temperature of the laser chip is kept constant by a controlled Thermo-Electric Cooler (TEC).

3 Detection scheme and evaluation algorithms with wide/narrow spectral scans

By filling the reference gas in the photodetector housing, a certain amount of absorption by methane is provided in any situation. Because of the large current to wavelength tuning range of more than 3 nm of the VCSEL, a broad wavelength range can be scanned to cover strong adjacent methane absorption lines (wide scan). These are used to identify the wavelength scale, so that the required laser current for the CO line wavelength position is known. The narrow spectrum scan covers a smaller wavelength interval to record the absorption line P8 of the first overtone vibrational band of CO.

The wide scan (Fig. 3) of about 3 nm every few seconds is used to identify the wavelength scale while more frequent narrow scans of 0.7 nm lasting 0.1 s (Fig. 6) are performed to determine the CO concentration using a linear least-squares curve fit.

3.1 Signal model for WMS

In wavelength modulation spectroscopy (WMS) the current of the laser diode is sinusoidally modulated around a bias

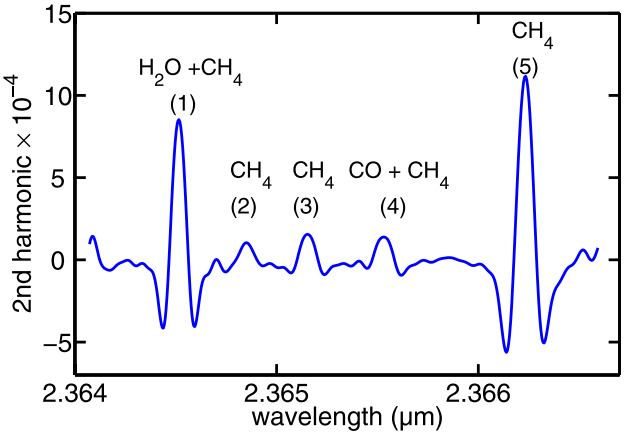

Fig. 3 Wide scan (duration: 640 ms, 512 samples): measured second harmonic spectrum of CO and CH_4 absorption lines. The wavelength scale is determined by the known wavelength positions of the two strong methane lines (1), (5) and either (3) or (4), depending on which line is larger

current $\overline{I}$ with a modulation frequency f_m and a current modulation amplitude I_A:

$$I(t) = \overline{I} + I_A \cos(2\pi f_m t). \tag{1}$$

The current causes a wavelength variation of

$$\lambda(t) = \overline{\lambda} + \lambda_A \cos(2\pi f_m t + \phi), \tag{2}$$

where λ_A is the wavelength modulation amplitude and ϕ is the phase shift between the wavelength and current variation. For small current variations around a bias point, the differential current to wavelength tuning behavior is linear [13], so we have

$$\lambda_A = \left.\frac{d\overline{\lambda}}{d\overline{I}}\right|_{\overline{I}} \cdot I_A \cdot \eta(f_m). \tag{3}$$

$\eta(f_m)$ is the frequency dependency of the current-to-wavelength tuning coefficient [13–15]. The wavelength modulated (FM) light passes through the gas to be measured, which absorbs light at specific wavelengths and the resulting amplitude/intensity modulated (AM) signal is detected with a photodetector. The Fourier coefficients of the AM signal at wavelength $\overline{\lambda}$ are selected with a lock-in amplifier. The second harmonic spectrum S_2 is defined as the 2nd Fourier coefficient as a function of $\overline{\lambda}$.

$$S_2(\overline{\lambda}) = \frac{1}{\pi}\int_{-\pi}^{\pi} T\left(\overline{\lambda} + \lambda_a \cos(z)\right)\cos(2z)\,dz, \tag{4}$$

with $z = 2\pi f_m t$ and $T(\lambda)$ the transmission function given by gas absorption line profiles according to the Lambert–Beer law. If the gas absorption line has a Lorentzian shape (atmospheric pressure) with an absorbance of less than 10%, the following approximation can be made for a single line:

$$T(\lambda) \approx 1 - \frac{a \cdot C \cdot l}{1 + \left(\frac{\lambda - \lambda_0}{\alpha_L}\right)^2}, \tag{5}$$

where a is the absorption coefficient at the absorption line center λ_0 [9], C is the gas concentration and l is the optical path length. For this case, $S_2(\overline{\lambda})$ has an analytic form given by Arndt ((27) in [16]), which is written with the parameters wavelength and modulation amplitude normalized to the absorption line HWHM α_L (HWHM: half-width at half-maximum).

3.2 Signal normalization

In the sensor the second harmonic output of the lock-in amplifier is normalized with the incident laser power for each spectral point separately to obtain a measurement of the second harmonic spectrum. No assumption on the shape of the laser PI characteristic is made, e.g. an assumption on threshold current, slope, etc. It is assumed that the zeroth harmonic signal equals the incident laser power. The influences of possible stray light and also strong absorption features are therefore neglected. These, however, are not considered as constrictions: the stray light power density needs to be as high as 4 W/m^2 (in the range 1.2 μm to 2.6 μm) on the detector surface to cause only 1% *relative error* on the concentration values. If the presence of stray light cannot be excluded by sensor design, the stray light intensity can be determined after the scan by employing an on-off modulation of the laser. Very strong absorption features with absorbance in the order of 10^{-2} also cause a maximum *relative error* of 1% on the concentration values, because of incorrect normalization. This effect, however, is deterministic and can be compensated if measurement of very high concentrations is needed.

3.3 Wide scan: determination of the current to wavelength tuning behavior

It was shown in [15] that the current-to-wavelength tuning behavior of VCSELs can be described with a second order polynomial. In the wide scan, at least three gas absorption lines (either CH_4 and/or CO) are used to determine the linear and quadratic current to wavelength tuning behavior (c_0, c_1, c_2):

$$\overline{\lambda}(\overline{I}) = c_2 \cdot (\overline{I} - I_0)^2 + c_1 \cdot (\overline{I} - I_0) + c_0 \tag{6}$$

with I_0 being an arbitrary but fixed current. The two strong methane lines (absorption curves 1, 5 in Fig. 3) on both sides of the CO line are always used. The consideration of the quadratic term c_2 is necessary for exact determination of the wavelength scale and the wavelength modulation amplitude,

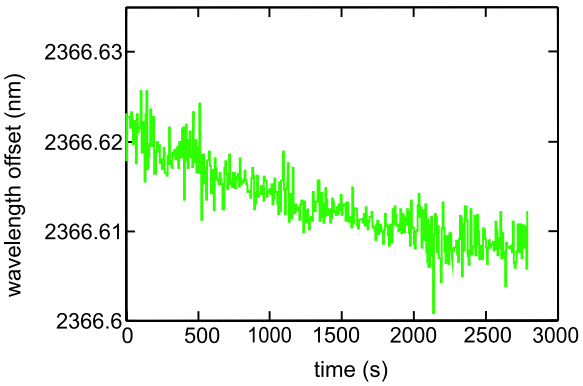

Fig. 4 Wavelength offset c_0 in variation of time: 10 pm wavelength shift in about 1 hour, which corresponds to a third of the HWHM of the gas absorption line

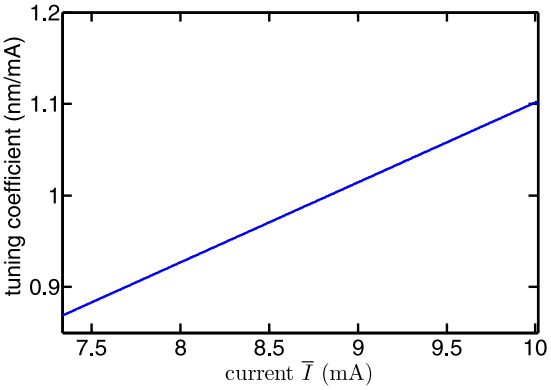

Fig. 5 The current-to-wavelength tuning coefficient $d\overline{\lambda}(\overline{I})/d\overline{I}$ in dependency of the bias current $\overline{I}$ obtained from (6)

which are needed for the computation of the reference spectra for the narrow scan. A variation of the coefficients (c_0, c_1, c_2) is caused by the laser aging, heat sink (T_s) or ambient temperature (T_{amb}) changes, i.e. $c_0 = c_0(T_{\text{amb}}, T_s, t)$. An example is given in Fig. 4. Although the laser heat sink temperature (T_s) is controlled by the TEC to be a constant, there is still an influence of the air temperature (T_{amb}) on the laser chip. This is because the temperature sensor, which gives a feedback to the TEC, measures the laser chip temperature not directly, but the submount temperature next to the laser chip. Furthermore, a drift of the temperature sensor characteristics may also contribute to the variation of c_0. Besides the wavelength scale, exact knowledge of the modulation amplitude λ_A is necessary for the exact computing of the reference spectra. Inserting (6) in (3):

$$\frac{\lambda_A}{I_A} = \left(2 \cdot c_2(\overline{I} - I_0) + c_1\right) \eta(f_m). \tag{7}$$

The tuning coefficient λ_A/I_A (see (3)) increases with bias current $\overline{I}$ as shown in Fig. 5 and typically decreases with modulation frequency f_m. c_1 and c_2 are determined during the wide scan. $\eta(f_m)$ cannot be assumed to be one, especially if the modulation frequency f_m is above or near the 3 dB cutoff frequency of the thermal tuning—for VCSELs the relevant cutoff frequency is several kHz to 100 kHz. In this case, we determine λ_A additionally from the distance between the zero crossings of the measured second harmonic spectrum λ_Z. λ_Z is mainly determined by λ_A, not the absorption line half-width α_L. By knowing α_L from HITRAN database with known gas temperature and pressure, there is an implicit relationship between λ_Z and the modulation amplitude λ_A [17]. In [18] this fact was even used to characterize the frequency modulation response of a laser diode. Therefore, by determining the λ_Z of the second harmonic spectrum of the two strong methane lines, λ_A can also be determined. By comparing these values and the value given by (7), $\eta(f_m)$ can be calculated.

When calculating the reference spectra for the narrow scan, λ_A is interpolated from Fig. 5 and scaled with $\eta(f_m)$. Furthermore, the gas pressure and temperature are assumed to stay constant between two wide scans. Gas pressure and temperature are either known or measured by a separate sensor.

3.4 Narrow scan: CO concentration determination with linear curve fit

For the determination of the CO concentration, a simple and fast algorithm is required, which provides the highest possible signal to noise ratio.

Because of the known wavelength scale determined from the wide scan, a non-iterative linear least-squares curve fit can be applied with analytically computed second harmonic reference spectra of CO and CH_4 absorption lines by using the Lorentzian line shape model [16] with parameters from the HITRAN database [9]. The linear least-squares algorithms can only be used if the unknown parameters are linear to the model function. If the model contains nonlinear parameters like gas temperature and pressure, nonlinear least-squares algorithms are to be used.

The measured second harmonic spectrum (narrow scan) $\mathbf{y} = (y_1, \ldots, y_N)^T$ (Fig. 6) consists of N samples. The signal model for $\mathbf{y}$ is linearly composed by four components (Fig. 7): second harmonic spectrum of CO, second harmonic spectrum of CH_4, a slope and an offset. The latter two items are due to laser residual amplitude modulation (RAM) [19]) caused by the nonlinear current–intensity modulation behavior (PI characteristic) of the laser. An offset and a slope in the second harmonic spectrum are caused by the second and third order components of the laser PI curve. The other small influences of RAM as described in Ref. [19], i.e. the presence of a first and third harmonic spectrum in the measured spectrum are neglected. The linear signal model for mea-

surement vector $\mathbf{y}$ is:

$$\mathbf{y} = \underbrace{(\psi_1|\psi_2|\psi_3|\psi_4)}_{\mathbf{\Psi}} \begin{pmatrix} C_{\mathrm{CO}} \cdot a \cdot l \\ C_{\mathrm{CH_4}} \cdot a \cdot l \\ l_o \\ l_s \end{pmatrix} + \epsilon \tag{8}$$

with

$$\mathrm{var}(\epsilon) = \sigma^2 \mathbf{I}, \qquad E(\epsilon) = 0, \tag{9}$$

where ϵ is white noise on $\mathbf{y}$ and $\mathbf{I}$ is the identity matrix. σ^2 is the noise power of the measurement spectrum and $E(\epsilon)$ denotes the expectation value of ϵ. $\mathbf{\Psi}$ is the component matrix with each column representing the components forming the measured spectrum:

$$\psi_1 = \left(S_2^{\mathrm{CO}}(\lambda_1), \ldots, S_2^{\mathrm{CO}}(\lambda_N)\right)^T, \quad \text{(target spectrum)} \tag{10}$$

$$\psi_2 = \left(S_2^{\mathrm{CH_4}}(\lambda_1), \ldots, S_2^{\mathrm{CH_4}}(\lambda_N)\right)^T, \quad \text{(interfering spec.)} \tag{11}$$

$$\psi_3 = (1, \ldots, 1)^T, \quad \text{(offset)} \tag{12}$$

$$\psi_4 = (-1, \ldots, 1)^T. \quad \text{(slope)} \tag{13}$$

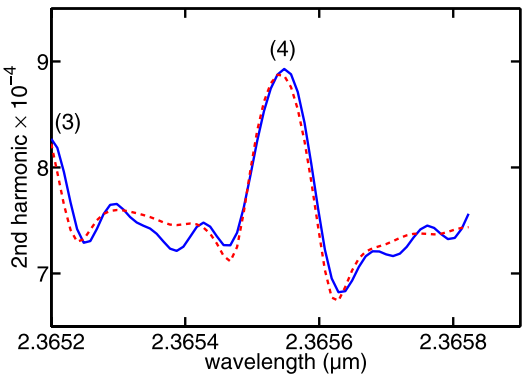

Fig. 6 Narrow scan (duration: 100 ms, 64 samples): second harmonic spectrum of CO and CH_4 absorption lines (*solid curve*), and the analytically computed and fitted reference curve (*dashed curve*). The CO absorption corresponds to 10 ppm m (c = 100 ppm, l = 10 cm)

The wavelength points λ_i are obtained when equally spaced bias current values are inserted in (6). The modulation amplitude—given by (7)—is dependent on the bias current value and thus is different for each component of ψ_1 and ψ_2. To improve readability, this fact is suppressed in (10) and (11). S_2^{CO} and $S_2^{\mathrm{CH_4}}$ are normalized second harmonic spectra where the peak CO absorbance value is scaled to one. The determination of the gas concentration thus works as follows: the direct result of the curve fit gives the spectral peak height in terms of absorbance. This is then divided by a and the optical path length l to obtain the gas concentration in ppm. Therefore, $\mathbf{\Psi}$ gives a pure measure of the curve fit independent of the line strength of CO gas absorption and the optical path length.

The parameters are the CO and CH_4 concentration ($C_{\mathrm{CO}}/C_{\mathrm{CH_4}}$), and the slope ($l_s$) and offset ($l_o$). There are more than 20 individual methane absorption lines in this spectral region having a peak absorption coefficient larger

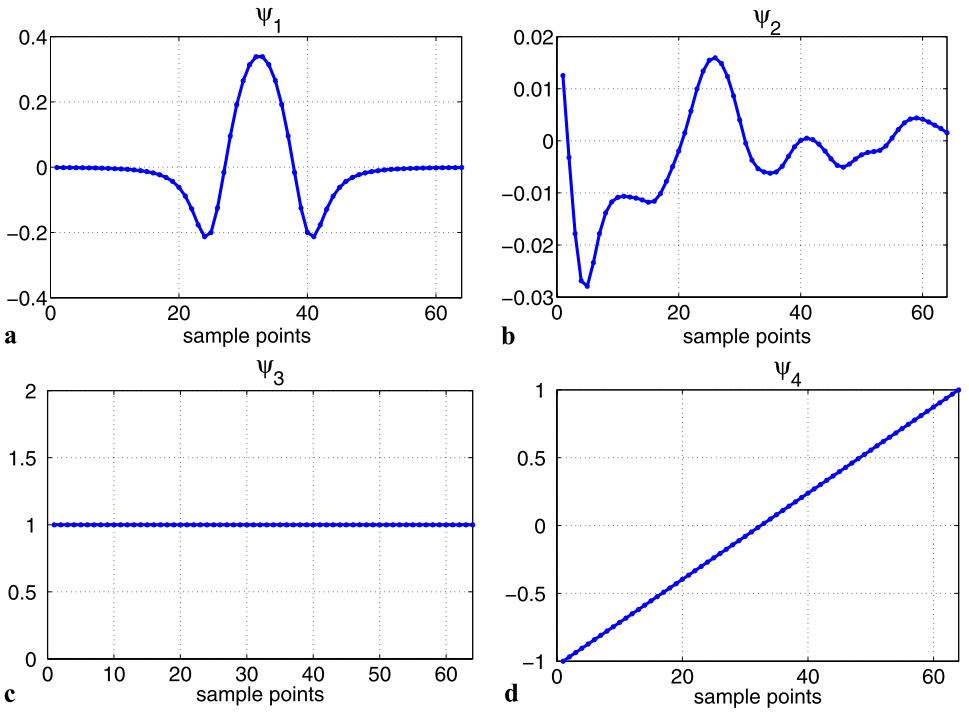

Fig. 7 The components of the model for curve fitting: (**a**) ψ_1, the second harmonic spectrum of CO at 2.365 nm with (**b**) interfering gas methane ψ_2 (second harmonic spectrum of 20 methane lines), (**c**) ψ_3 and (**d**) ψ_4 are the spectral baseline: offset and slope

than 10^{-6} and are taken into consideration in the calculation. The sum of the methane absorbance at the CO line center is about 20% of the contribution of the CO line at the same concentration. 1 ppm m CO corresponds to a peak absorbance of $3.6 \cdot 10^{-5}$.

The linear least-squares curve fit, which minimizes the squared difference between $\mathbf{y}$ and the model function, has the optimal solution for the parameters as follows [20]:

$$\begin{pmatrix} \widehat{C}_{\mathrm{CO}} \cdot a \cdot l \\ \widehat{C}_{\mathrm{CH_4}} \cdot a \cdot l \\ \widehat{l}_o \\ \widehat{l}_s \end{pmatrix} = \left(\mathbf{\Psi}^T \mathbf{\Psi}\right)^{-1} \cdot \mathbf{\Psi}^T \mathbf{y}. \tag{14}$$

The estimated parameters are denoted with a hat accent and are given by the scalar product of the scan vector $\mathbf{y}$ and the pseudo inverse of $\mathbf{\Psi}$ matrix. The CO concentration therefore is calculated by a scalar product, which is appropriate to micro-controller programming because it is very efficient. A sample result of the curve fit is shown in Fig. 6.

3.5 Narrow scan: optimum scan width for optimization of SNR on the estimated concentration

The wide scan could be in principle utilized both for the identification of the wavelength scale, and also for the determination of the gas concentration value, in which case, however, the noise on the estimated CO concentration is not minimized. In this section, we investigate the optimized scan width both theoretically and experimentally. In the section on experimental results Sect. 4.1 an Allan plot of the sensor is presented, that clearly shows a dominating white noise behavior for sensor averaging times below 1 s. Due to the high measurement rate of 10 Hz (averaging time 0.1 s) the sensor is white noise limited. Therefore, in this section only white sensor noise is treated. A formula for the standard deviation of the concentration noise $\sigma(\widehat{C}_{\mathrm{CO}})$ derived from (14) is given by (14) in [21], which also is the sensor sensitivity:

$$\sigma(\widehat{C}_{\mathrm{CO}}) = \sigma_0 \sqrt{\left(\mathbf{\Psi}^T \mathbf{\Psi}\right)^{-1}_{11} N} \tag{15}$$

with

$$\sigma_0 = \frac{1}{a\,l} \sqrt{S_{yy}\, R}, \tag{16}$$

$\left(\mathbf{\Psi}^T \mathbf{\Psi}\right)^{-1}_{11}$ is the left top element of the inverse matrix of $\mathbf{\Psi}^T \mathbf{\Psi}$. As clearly can be seen, $\sigma(\widehat{C}_{\mathrm{CO}})$ (unit: ppm) is a function of

- $\left(\mathbf{\Psi}^T \mathbf{\Psi}\right)^{-1}_{11} N$ (unit: 1): measure of the noise attenuation by the curve fit. It depends on the signal model.
- S_{yy} (unit: Hz^{-1}): the noise power density on the measurement data $\mathbf{y}$ in terms of absorbance.
- R (unit: Hz): the measurement rate of gas concentration.
- a (unit: $(\mathrm{ppm\,m})^{-1}$): peak absorption coefficient of the target gas CO in the wavelength scanning range of the laser.
- l (unit: m): optical path length.

When $\sigma(\widehat{C}_{\mathrm{CO}})$ is normalized to σ_0, it is not dependent on the absorption line strength, the absorption path length, the system noise level as well as the measurement rate. It is thus a pure measure for the noise attenuation by the curve fit. Note that $\left(\mathbf{\Psi}^T \mathbf{\Psi}\right)^{-1}_{11} N$ is constant for $N \to \infty$, because $\left(\mathbf{\Psi}^T \mathbf{\Psi}\right)^{-1}_{11}$ is asymptotically inversely proportional to N, where the limiting case also represents the continuous situation without sampling.

If a low pass filter is utilized before the curve fit to filter the measurement noise of $\mathbf{y}$, the standard deviation of gas concentration noise can be written as:

$$\sigma(\widehat{C}_{\mathrm{CO}}) = \sigma_0 \sqrt{N} \left| \left(\left(\mathbf{\Psi}^T \mathbf{\Psi}\right)^{-1} \mathbf{\Psi}^T \right)_1 * h \right|. \tag{17}$$

The * denotes the convolution operator. $(X)_1$ specifies the first row of a matrix X. h is the impulse response of the low pass filter with its mean square value $|h|$ normalized to one. Because of convolution with h (17) cannot be simplified anymore to (15).

The smaller $\sigma(\widehat{C}_{\mathrm{CO}})/\sigma_0$ is, the better is the performance of the curve fit. This value can be optimized by changing the width of the narrow spectrum scan. In this case, the ψ vectors are different with respect to the sampled points $(1 \ldots N)$. The normalized standard deviation $\sigma(\widehat{C}_{\mathrm{CO}})/\sigma_0$ versus the width of the narrow scan is shown in Fig. 8. The curve with red dots shows the experimental result, while the blue curve represents the theory given by (17). In the theory, h is the impulse response of an analog Bessel filter second order with cutoff frequency of 100 Hz, while in the measurement system it is included as an analog low pass before sampling. The optimal sampling width in this case is 9 times HWHM of the CO absorption line. The improvement over a scan with width of 20 times HWHM is about 33%. The good agreement of experiment and theory proves the applicability of the theory, so it can also be applied for other spectral regions as well.

4 Sensor characterization and sensing result

The sensor was characterized with an Allan variance plot and tested for fire detection as well as for combustion optimization in the exhaust gas pipe of a gas furnace.

4.1 Allan variance plot

Under controlled temperature (30°C) and pressure (960 mbar), a one-day measurement was carried out to characterize the system performance. The CO concentration is

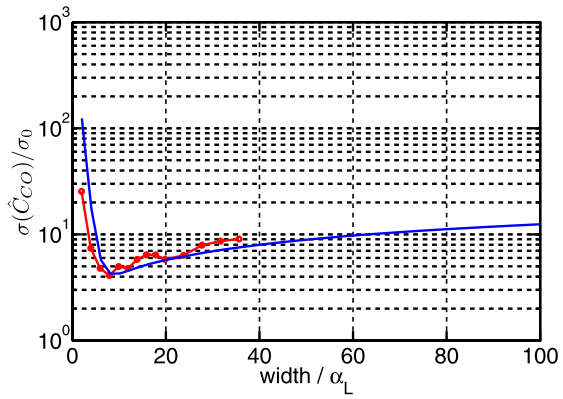

Fig. 8 Normalized standard deviation $\sigma(\widehat{C}_{\mathrm{CO}})/\sigma_0$ versus width of the narrow scan: experimental results (*curve with red dots*) show good agreement with theory (*blue curve*). The width of the narrow spectrum scan is normalized to the HWHM of the CO absorption line (α_L). The width of the wide scan shown in Fig. 3 is about 100 times α_L, and the optimum scan width for narrow scan should be at the minimum of the curve: 9 times α_L

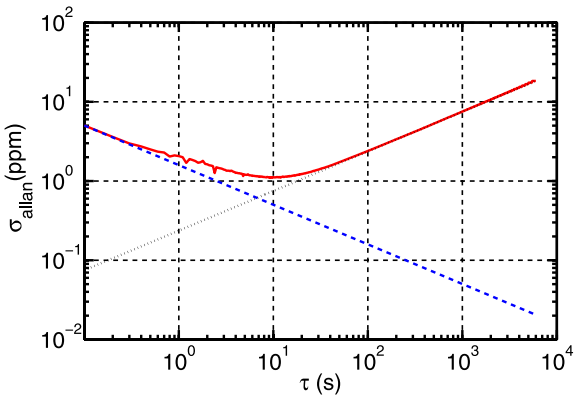

Fig. 9 The Allan standard deviation σ_{allan} as a function of the averaging time τ (*solid line*). It consists of three components: τ^{-1} (*dashed line*), τ^0 and τ^1 (*dotted line*), which indicate the existence of the white noise, pink noise ($1/f$ noise) and red noise ($1/f^2$ noise), respectively

determined every 100 ms. By averaging the CO concentration, the standard deviation decreases. The standard deviation of the CO estimation is 2 ppm with 1 s time resolution. This corresponds to an absorbance of $1 \cdot 10^{-5}$.

The Allan variance plot [22] is shown in Fig. 9, which can be divided into three parts: τ^{-1}, τ^0 and τ^1, the two latter term indicate the existence of the pink noise ($1/f$ noise) and red noise ($1/f^2$ noise) [23]. The optimum integration time τ_{opt}, where the Allan variance curve is minimum, is approximately 12 s. It is not clear what the cause of the observed drift is. It could be an instability in the optical cell, which can be handled by improving the optical setup. Alternatively, the accuracy of the wavelength stabilization may be still too low. Since the repetition rate of the wavelength stabilization of 6 s is far below the time constant of the wavelength drift (see Fig. 4), averaging will substantially enhance

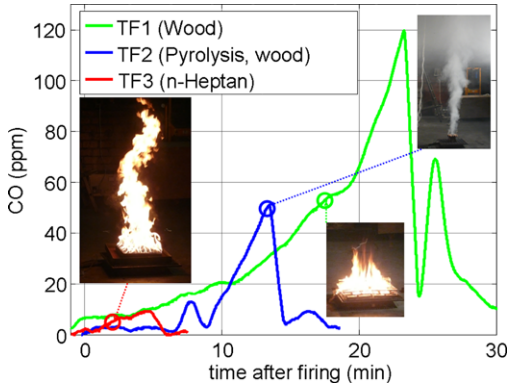

Fig. 10 Measurement results of different test fires (TF) with one minute integration time. Pyrolysis (TF2) is burning with lack of oxygen. All of the fires are detected. The steep concentration drop results from the ventilation of the room

the wavelength scale accuracy. Furthermore, background instabilities of the first available sample lasers may also have some impact on the observed drift.

4.2 Fire detection

To carry out fire detection tests according to the European Standard EN 54 [24], the sensor gas inlet is mounted at the ceiling of a room on a 3 m radius circle around the test fire. The purging after the end of the test fire is visible in Fig. 10 as a steep decrease in CO concentration. Since the room has a very high volume (228 m^3), the CO concentration stays below 120 ppm for the wood fire and the pyrolysis ("smoldering", e.g. wood on a hot plate). Pyrolysis is a very incomplete burning with no flame and very high CO generation (up to vol% range). Therefore, the CO concentration at pyrolysis increases much faster than the CO concentration produced by the wood fire. In case of open fires like n-heptane (Fig. 10), much less CO is generated. These kinds of fires are also typically more difficult ones to detect for smoke detectors, because of less particle generation.

4.3 CO concentration measurement in the exhaust gas of a furnace

CO measurement in the exhaust gas of gas furnaces is relevant for the optimization of the burning process. Usually detection of CO in the 10 ppm range is requested. When the furnace is turned on, a CO concentration peak occurs for approximately 2 s full-width at half-maximum (Fig. 11), which demonstrates the advantage of the high time resolution of the CO sensor.

5 Conclusion

We have achieved the first 2.3 µm VCSEL-based CO sensor. It uses a compact (7 cm overall extent feasible) absorption

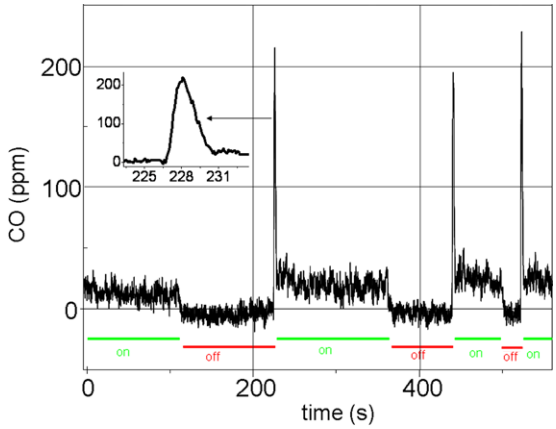

Fig. 11 A CO measurement in exhaust gas of a gas furnace: the burner is turned on and off frequently simulating the real operating condition. The CO peak could be measured in this application because of the very fast time resolution of 100 ms

cell with 10 cm optical path length capable of detecting CO with ppm resolution in 1 s (1 σ: 2 ppm). By using the photodetector housing as reference cell containing methane, a complex measurement setup with a separate reference cell for line locking is avoided. By utilizing a wide (wavelength scale identification)/narrow (CO concentration determination) spectrum scan concept, the sensor is calibration-free during its life time. Sensor malfunction, blockade of the optical path and the eventual outdiffusion of the reference gas can be detected. In the wide spectrum scan, an automated determination scheme of the nonlinear current-to-wavelength scale is implemented, with which the laser aging process can be monitored and compensated. Since the CO line position and the WMS wavelength modulation amplitude are very accurately known from the wide scan, an efficient linear least-squares algorithm with analytically calculated reference spectra is applied in the narrow spectrum scan for the CO concentration determination. Neither background measurement nor reference spectra measurements are needed. To perform an efficient curve fit, the scan width of the narrow scan is adjusted to 9 times of the gas absorption width, which enables an improvement of the detection sensitivity (1 σ) of 33% compared to a larger scan width of 20 HWHM. With this sensor, CH_4 can also be detected well in the wide scan with ppm resolution by knowing the exact absorbance of the reference gas in the photodetector; otherwise, the detection resolution of methane is limited by the uncertainty of the methane amount in the photodetector, which is still sufficient for some applications like exhaust gas monitoring in gas furnace or safety monitoring for explosion protection. The wide/narrow scan concept is universal and can also be used for sensing of other gases e.g. NO/H_2O and CO_2/H_2O using VCSELs at 1.8 µm and 2.0 µm, respectively. The concepts described in this paper allow for the realization of compact gas sensors and demonstrate how the specific properties of VCSELs can be used to improve laser optical gas sensors.

Further work will include employment of a higher accuracy signal model in the sensor to lower the already low cross-sensitivity to CH_4, which causes a slight offset of a few ppm for CO. This may include use of molecule parameters with higher accuracy and/or the inclusion of a more sophisticated model for laser RAM effects. Ultimate long-term stability can be expected as besides molecule parameters no further calibration factors are required.

Acknowledgements The authors would like to thank Marcel Thraenhardt for careful proof-reading and gratefully acknowledge the financial support by the Federal Ministry of Education and Research of Germany (Project 'NOSE', contract No. 13N8772) and by the European Union (Project 'NEMIS', contract No. 031845).

Appendix: Variables and definitions

Name	Unit	Def.
$\overline{I}$	A	laser bias current
$\overline{\lambda}$	nm	bias wavelength
$S_2(\lambda)$	1	second harmonic spectrum (second harmonic intensity divided by the DC light intensity)
f_m	Hz	modulation frequency
α_L	nm	absorption line width (HWHM)
C_{CO}	ppm	gas concentration of CO
l_o	1	offset of the spectral background
$\mathbf{y}$	1	measured second harmonic spectrum vector
ψ_i	1	spectral component vectors
N	1	number of points per narrow spectrum scan
h	1	impulse response of low pass filter (normalization $\|h\| = 1$)
I_A	A	current modulation amplitude
λ_A	nm	wavelength modulation amplitude
a	$(\text{ppm m})^{-1}$	peak absorption coefficient of the probed line
λ_0	nm	center wavelength of the probed line
l	m	optical path length
C_{CH_4}	ppm	gas concentration of methane
l_s	1	slope of the spectral background
S_{yy}	1/Hz	the noise power density on $\mathbf{y}$
$\mathbf{\Psi}$	1	component matrix (columns ψ_i)
R	Hz	measurement rate
σ_0	ppm	normalization factor for the noise on the measured gas concentration $\sigma(\widehat{C}_{CO})$

References

1. Center for Disease Control and Prevention, Online electronic publication: http://www.cdc.gov/co/faqs.htm (2007)

2. R. Pohle, E. Simon, R. Schneider, M. Fleischer, R. Sollacher, H. Gao, K. Müller, P. Jauch, M. Loepfe, H.-P. Frerichs, C. Wilbertz, Sens. Actuators, B, Chem. **120**, 669 (2007)
3. J.-C. Nicolas, A.N. Baranov, Y. Cuminal, Y. Rouillard, C. Alibert, Appl. Opt. **37**, 7906 (1998)
4. A. Vicet, D. Yarekha, A. Pérona, Y. Rouillard, S. Gaillard, A. Baranov, Spectrochim. Acta Part A **58**, 2405 (2002)
5. H. Teichert, T. Fernholz, V. Ebert, Appl. Opt. **42**, 2043 (2003)
6. V. Ebert, H. Teichert, P. Strauch, T. Kolb, H. Seifert, J. Wolfrum, Proc. Combust. Inst. **30**, 1611 (2005)
7. J. Wang, M. Maiorov, D.S. Baer, D.Z. Garbuzov, J.C. Connolly, R.K. Hanson, Appl. Opt. **39**, 5579 (2000)
8. J. Seufert, M. Fischer, M. Legge, J. Koeth, R. Werner, M. Kamp, A. Forchel, Spectrochim. Acta Part A, Mol. Biomol. Spectrosc. **60**, 3243 (2004)
9. L. Rothman, D. Jacquemart, A. Barbe, D.C. Benner, M. Birk, L. Brown, M. Carleer, C. Chackerian, Jr., K. Chance, L. Coudert, V. Dana, V. Devi, J.-M. Flaud, R. Gamache, A. Goldman, J.-M. Hartmann, K. Jucks, A. Maki, J.-Y. Mandin, S. Massie, J. Orphal, A. Perrin, C. Rinsland, M. Smith, J. Tennyson, R. Tolchenov, R. Toth, J.V. Auwera, P. Varanasi, G. Wagner, J. Quant. Spectrosc. Radiat. Transfer **96**, 139 (2005)
10. M. Ortsiefer, G. Böhm, M. Grau, K. Windhorn, E. Rönneberg, J. Rosskopf, R. Shau, O. Dier, M.-C. Amann, Electron. Lett. **42**, 640 (2006)
11. G. Böhm, M. Grau, O. Dier, K. Windhorn, E. Rönneberg, J. Rosskopf, R. Shau, R. Meyer, M. Ortsiefer, M.-C. Amann, J. Cryst. Growth **301**, 941 (2007)
12. A. Bachmann, K. Kashani-Shirazi, T. Lim, O. Dier, C. Lauer, M.-C. Amann, in *20th International Conference on Indium Phosphide and Related Materials*, Versailles, France, 2008
13. J. Chen, A. Hangauer, R. Strzoda, M.-C. Amann, Appl. Phys. Lett. **91**, 141105 (2007)
14. S. Schilt, L. Thévenaz, Appl. Opt. **43**, 4446 (2004)
15. A. Lytkine, W. Jaeger, J. Tulip, Spectrochim. Acta Part A **63**, 940 (2006)
16. R. Arndt, J. Appl. Phys. **36**, 2522 (1965)
17. J. Reid, D. Labrie, Appl. Phys. B, Lasers Opt. **26**, 203 (1981)
18. J. Chen, A. Hangauer, R. Strzoda, M.-C. Amann, Appl. Phys. B, Lasers Opt. **90**, 243 (2008)
19. P. Kluczynski, J. Gustafsson, Å.M. Lindberg, O. Axner, Spectrochim. Acta Part B, At. Spectrosc. **56**, 1277 (2001)
20. A. Bjorck, *Numerical Methods for Least Squares Problems* (Society For Industrial and Applied Mathematics, Philadelphia, 1996)
21. J. Chen, A. Hangauer, R. Strzoda, M.C. Amann, Appl. Phys. B, Lasers Opt. **100** (2010). doi:10.1007/s00340-010-3973-2
22. D.W. Allan, Proc. IEEE **54**, 221 (1966)
23. P. Werle, R. Muecke, F. Slemr, Appl. Phys. B **57**, 131 (1993)
24. European Standard, *EN54-26: Fire Detection and Fire Alarm Systems—Part 26: Point Fire Detectors Using Carbon Monoxide Sensors* (Beuth, Berlin, 2008)